A 2 Degree of Freedom Dynamical System for Interdecadal Oscillations of the Ocean–Atmosphere

ALAIN COLIN DE VERDIÈRE

Laboratoire de Physique des Océans, Université de Bretagne Occidentale, Brest, France

THIERRY HUCK

Princeton University, and Geophysical Fluid Dynamics Laboratory, Princeton, New Jersey

(Manuscript received 11 February 1999, in final form 23 July 1999)

ABSTRACT

A four-box model of the ocean–atmosphere is constructed that exhibits self-sustained oscillations in the regime of decadal to interdecadal periods found in oceanic general circulation models under certain boundary conditions. The oscillations are assumed to be caused by a type of baroclinic instability that relies on the store of available potential energy in the ocean. To represent this process in a low-order model, the authors propose Landau's equation to govern the evolution of the overturning branch of the oceanic circulation. The domains of the unstable oscillations are found from linear stability analysis, and the nonlinear regimes are explored numerically. On these long timescales the atmospheric temperatures follow the oceanic temperatures. If the atmospheric temperatures are forced to be constant, the oscillations become strongly damped and disappear. The implications of the simple physics of this model for the decadal oscillations observed in more complex two- or three-dimensional GCMs are discussed.

1. Introduction

The North Atlantic oscillation (NAO) is the best example of the existence of climate variability on the decadal timescale (Hurrell and van Loon 1997). The good correlation between the strength of the westerlies and the large-scale sea surface temperature (SST) anomalies in the North Atlantic shows that both the atmosphere and ocean are active in the oscillations and the basic question, unanswered so far, is whether the decadal modulation of the NAO is an internal mode of the atmosphere with the ocean reacting passively, the converse, or neither (i.e., intrinsically coupled modes). Because decadal timescales are in the range of periods of free oceanic waves (baroclinic Rossby waves suitably modified to take into account the existence of an underlying mean circulation), it is likely that the ocean plays a central role. Indeed surface observations in the North Atlantic suggest enhanced variability for quasi-decadal and 40–60-yr periods (Deser and Blackmon 1993; Kushnir 1994), in which the ocean circulation contributes actively; Sutton and Allen (1997) show the coherent propagation of SST anomalies along the Gulf Stream and North Atlantic Current paths across the basin on decadal timescales, while Delworth and Mann (2000) discuss the role of the thermohaline circulation in the multidecadal oscillations found over the last 300 yr of reconstructed surface temperatures from proxy data (Mann et al. 1998).

Over the last 10 yr, numerous simulations of the large-scale ocean circulation under boundary conditions of given flux at the air–sea interface, for at least one of the temperature or salinity variables, show unequivocally that decadal oscillations are generic features of the oceanic model response (Cai et al. 1995; Capotondi and Holland 1997; Greatbatch and Peterson 1996; Greatbatch and Zhang 1995; Huang and Chou 1994; Huck et al. 1999a, hereinafter HCW; Weaver and Sarachik 1991; Weaver et al. 1993; Winton 1996). As the diffusion or surface flux sensitivity to SST are sufficiently lowered (Chen and Ghil 1996; Colin de Verdière and Huck 1999, hereinafter CVH), they appear spontaneously in the form of large-scale surface-intensified thermal anomalies of a few degrees. They are more intensified in the northern part of basins and are associated with fluctuations in the western boundary current transport and global overturning of several Sverdrups. CVH suggested that the cause of these oscillations is the baroclinic instability of the mean state in the region of strongest surface heat losses. These multidecadal modes may re-

Corresponding author address: A. Colin de Verdière, Laboratoire de Physique des Océans, Université de Bretagne Occidentale, 6 avenue Le Gorgeu, B.P. 809, 29285 Brest Cedex, France.
E-mail: acolindv@univ-brest.fr

semble the observed mode, as well as the Geophysical Fluid Dynamics Laboratory R15 coupled model oscillation (Greatbatch and Zhang 1995). Although a realistic North Atlantic configuration and forcing may or may not oscillate under constant flux and then require atmospheric stochastic forcing (Delworth and Greatbatch 2000; Griffies and Tziperman 1995), the ultimate pattern and period are set by the ocean circulation and require an understanding per se.

When the oscillations are nearly monochromatic, two variables are necessary for the existence of the oscillatory states. We need then to derive model equations for these two variables that may reproduce the physics present in models of higher complexity. Stommel (1961) pioneered this approach to show that a two-box ocean model with overturning proportional to density differences between the boxes could exhibit multiple steady states provided that temperature and salinity were restored to surface values with different time constants. This suggestion of the existence of multiple states in ocean general circulation model (OCGM) and box models of increased complexities was explored by Bryan (1986), Marotzke (1990), Weaver et al. (1993), Marotzke and Willebrand (1991), and many others in the context of mixed boundary conditions (i.e., restoring the temperature and flux on salinity).

Decadal oscillations were first observed in such simulations by Weaver and Sarachik (1991), who suggested an advective mechanism. However, a fluid with two components of state is not necessary as fixed flux experiments with either salinity (Huang and Chou 1994) or temperature alone (Greatbatch and Peterson 1996; Greatbatch and Zhang 1995; HCW) (demonstrated later). Many authors used 2D OGCMs and none reported decadal oscillations (see Winton 1996) until recently (Drbohlav and Jin 1998). Prior to this last study, the dynamics used in these models were roughly speaking similar to those used by Stommel with friction (acting on meridional velocity) balancing the meridional pressure gradient with ad hoc coefficients to take into account some effects of the rotation. Realizing that the meridional circulation is not in equilibrium with the density field in the decadal oscillations observed in 3D models, Drbohlav and Jin turned to unsteady dynamics and let meridional accelerations respond to meridional pressure gradients. We will point out that the long-period oscillations that they obtain have very different physics from what happens in three dimensions.

Ruddick and Zhang (1996) revisited Stommel's box model and added some new features such as a nonlinear dependence of the overturning with density contrast and a temperature-dependent hydrological cycle, but they concluded that the model was unable to oscillate. Griffies and Tziperman (1995) proposed another box ocean model adding a separation between thermocline and abyssal waters to Stommel's original formulation. They showed the existence of a damped oscillatory mode about a thermally dominant state and proposed the idea that white noise atmospheric forcing of such a mode could be responsible for the variability found in the coupled climate model of Delworth et al. (1993). Even more ambitious box models have been put forward by Birchfield (1989)—coupling an energy balance model (EBM) of the atmosphere to a three-box ocean with active temperature and salinity components. He recovered Stommel's thermally and salinity-dominant states and discovered the existence of amplified century-long oscillations when the evaporation was sufficiently strong. This oscillatory state was transient as the system showed abrupt bifurcations to the salinity-dominant steady state. Welander (1982) was very inventive in the construction of simple fluid oscillators. He proposed one in 1982 made of a surface box that relaxed both values of T and S to prescribed values on different timescales and mixed to a large reservoir whenever surface density exceeded the density of the reservoir. These last examples need two components, T and S, to work and so cannot be directly relevant to the physics of one variable decadal oscillation, which is the subject of the present paper.

To summarize what has been done so far, it seems therefore that there is a need for a box model that would allow self-sustained oscillations in the regime of interdecadal periods and that does not require a two-component oceanic fluid (with different boundary conditions for temperature and salinity), because OGCMs oscillate with a single component fluid. Given the general complexity of GCMs, it is necessary to test ideas with simpler analogs that have a limited number of degrees of freedom and allow one to go up and down the scale of complexity with added focus on specific processes, whose physical understanding are prerequisites for climate predictability studies. Steps in this direction for decadal oscillations were made by CVH, who suggested, from a study of the linear perturbations of a four-box ocean–atmosphere model with heat exchanges only, that the perturbations could indeed oscillate provided 1) the existence of a phase lag between the overturning and the equator-to-pole temperature contrast and 2) an instability process sufficiently active to overcome the stabilizing effect of the diffusion. The above phase lag is indeed an observed feature in OGCM simulations (Greatbatch and Peterson 1996; HCW), and a number of supporting elements for the presence of an active baroclinic instability in OGCM simulations were brought forward by CVH. There was, however, a major hypothesis in their perturbations equations that neglected the advection of temperature anomalies by the mean flow. Although this damping term was shown to be small in an analysis of OGCMs simulations (HCW), the model could not be considered a complete physical analog of OGCM oscillations.

The objective of the present study is to reject CVH's hypothesis and bring an answer to this problem. We propose a 2 degree of freedom dynamical system that oscillates on decadal periods and ultimately rests on

plausible physical grounds. The evolution of temperature contrast obeys a heat transport equation identical with Stommel's (1961) formulation, but the equation for the overturning is different; its rate of change is made proportional to the product of the overturning itself and a measure of the available potential energy in the ocean. A frictional term is added to stabilize the system at large amplitudes. The equation is derived after an analysis in section 4 that demonstrates that the choices are severely limited if self-sustained oscillations are to exist under the constraints of a fixed external heat flux.

Section 2 recalls the salient features of the interdecadal oscillations in an OGCM coupled to a simple atmospheric energy balance model. In section 3, we discuss zonally averaged models, in particular we show that Drbohlav and Jin's (1998) two-dimensional oscillations have very special physics that do not qualify as good analogs of 3D oceanic oscillations. The solutions of the proposed box model are analyzed in sections 4 and 5; the stability analysis of the fixed points is performed and the properties of the oscillations in the nonlinear regime are found numerically. Some implications of these results for the decadal oscillations found in OGCMs are discussed in section 6; the detailed comparison with the results of the three-dimensional ocean model coupled to a one-layer energy balance model of the atmosphere (section 2) shows encouraging support for the box model parameterization at small amplitudes, but highlights significant differences in the nonlinear regime.

2. Oscillations in a three-dimensional coupled model

In order to provide a short description of the oscillations of the thermohaline circulation in an idealized coupled configuration, we set up a three-dimensional ocean model coupled to an atmospheric energy balance model. The ocean model is described in Huck et al. (1999b). The dynamical part is based on the planetary geostrophic equations with Laplacian horizontal viscosity ($A_H = 10^5$ m^2 s^{-1}) and no-slip boundary conditions, but no vertical viscosity (which would be negligible given the large horizontal diffusivity necessary to resolve the Munk boundary layer), no bottom friction or wind forcing (such that the barotropic mode in a flat-bottom basin is zero). The thermodynamical part is limited to the equation for temperature with a linear equation of state (the thermal expansion $\alpha = 2 \times 10^{-4}$ K^{-1}), including advection, diffusion (horizontal and vertical diffusivities are constant, respectively, 1000 and 10^{-4} m^2 s^{-1}), convection (as described by Rahmstorf 1993), and surface forcing. The equations are discretized on an Arakawa B grid in Cartesian coordinates, for a mid-latitude β-plane ocean basin centered at 40°N, extending from 20° to 60°N, 5120 km wide, and 4500 m deep. The resolution is relatively coarse: 160 km horizontally and 15 levels vertically (respectively, 50 × 3, 100, 150, 200, 250, 300, 350, 400, 450, 500, 550 × 3 m thick).

The atmospheric EBM is a one-layer atmosphere (heat capacity is 10^7 J m^{-2} K^{-1}), absorbing incoming solar shortwave radiation at the rate of 157 W m^{-2} × cos[π(latitude − 20°)/40°], such that the mean heating (cooling) is 100 W m^{-2} in the southern (northern) half of the domain, and radiating infrared to space as a linear function of its temperature ($B = 1.7$ W m^{-2} K^{-1}). The horizontal heat transport is parameterized as a diffusion law with a constant coefficient of 0.5×10^6 m^2 s^{-1}. The horizontal grid is identical to the ocean's, while the Euler time integration requires a much shorter time step (1 h). The exchange of heat between the atmosphere and the ocean is proportional to the difference between the atmospheric and oceanic surface temperature (exchange coefficient of 15 W m^{-2} K^{-1}). Geometry, parameterizations, and parameters are chosen to be as similar as possible to the box model analyzed later (sections 4 and 5).

The coupled integration spans 6000 yr (the initial temperature field is uniformly 5°C), starting with large amplitude oscillations that slowly weaken and settle into constant amplitude. The mean overturning (Fig. 1) is then 10 Sv (1 Sverdrup = 10^6 m^3 s^{-1}), with a standard deviation of 0.5 Sv, realizing a mean poleward heat transport close to 0.5 PW (1 PW = 10^{15} W). Meanwhile, the temperature difference between the upper 850-m southern and northern half ocean boxes varies by 0.1° around 3.7°C. The oscillation period is then very close to 20 yr. Within such a small amplitude regime, the oscillations are very smooth and regular (Fig. 2), but not perfectly sinusoidal though. The meridional overturning rises very linearly on a 14-yr time-scale but drops more sharply within the next 5 yr. Although not as asymmetric, the temperature difference between the upper boxes starts rising 3 yr before the overturning, peaks 5 yr after it started, and declines more smoothly for the remaining 12 yr. These asymmetries are stronger when the amplitudes are larger in the early centuries of the coupled run; however, in the small amplitude regime the oscillations behave quasi-linearly.

The variability is concentrated in the northern half of the basin, especially in the western regions, in the ocean as well as in the atmosphere (Figs. 3a,c). The standard deviation of the surface fluxes during the oscillations remains small in comparison with the time-averaged values (Fig. 3b), supporting the use of constant flux in previous experiments (Greatbatch and Zhang 1995; HCW; CVH). We show different phases of an oscillation for the zonally averaged temperature and meridional overturning (Fig. 4). The variability remains localized in the upper 500 m of the ocean, especially in the northern regions. Temperature anomalies follow closely changes in the thermohaline circulation, although it is hard to understand the origin of the oscillations in these zonally averaged quantities, provided mainly for com-

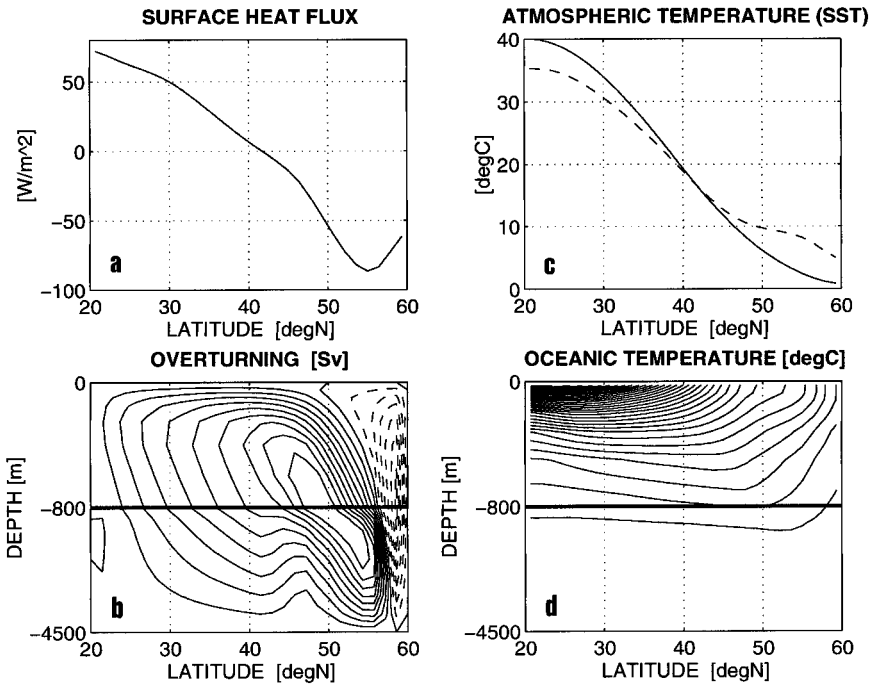

FIG. 1. The 3D coupled model climatology: (a) time- and zonally averaged surface heat flux, (b) overturning (contours every Sverdrup, dashed lines are negative contours), (c) atmospheric temperature (solid) and SST (dashed), and (d) oceanic stratification (contours every 1 °C).

parison with oscillations in 2D models (Drbohlav and Jin 1998).

The oscillatory behavior has its roots in the phase lag between overturning and meridional density gradient on decadal timescales (Fig. 2), because of the adjustment of the thermohaline circulation through baroclinic planetary waves that propagate across the basin in several years to decades. However, the source of energy that sustains the oscillations against dissipation is the long-wave baroclinic instability of the currents and stratification structure in the northwestern region of the domain—we refer the reader to previous analysis of the oscillations in very similar settings for the detailed arguments that lead us to these conclusions (HCW; CVH).

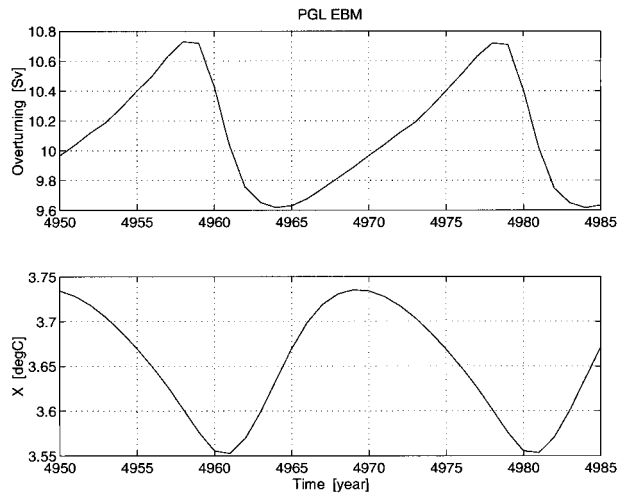

FIG. 2. Time evolution of the maximum overturning and the south–north temperature contrast in the upper 850 m (the box model–type variables) for the 3D coupled PGL–EBM model oscillations. Note the slow rise (rapid decline) of the overturning and the opposite situation for the temperature contrast.

3. Zonally averaged model analog?

Many of the OGCMs that have been run with flux boundary conditions exhibit decadal oscillations that do not depend on a two-component (T, S) fluid and the present single-component (T) model illustrates the baroclinic instability mechanism and the oscillations it triggers in its simplest form. The rather passive role of the atmosphere on these long timescales, given the choice of representative parameters of the present climate system that we have used, suggests that there is no reason for the same mechanism not to operate in more complex coupled ocean–atmosphere circulation models. As in Landau's early work on the genesis of the turbulence, the major difficulty is to derive the equation for the overturning from the hydrodynamical equations of motions in zonally averaged models. Past efforts in this direction include those of Marotzke et al. (1988), Wright and Stocker (1991), Wright et al. (1995), and Winton (1996). They derived equations for the overturning in the spirit of Stommel's 1961 formulation equilibrating buoyancy torque and friction. These two-dimensional

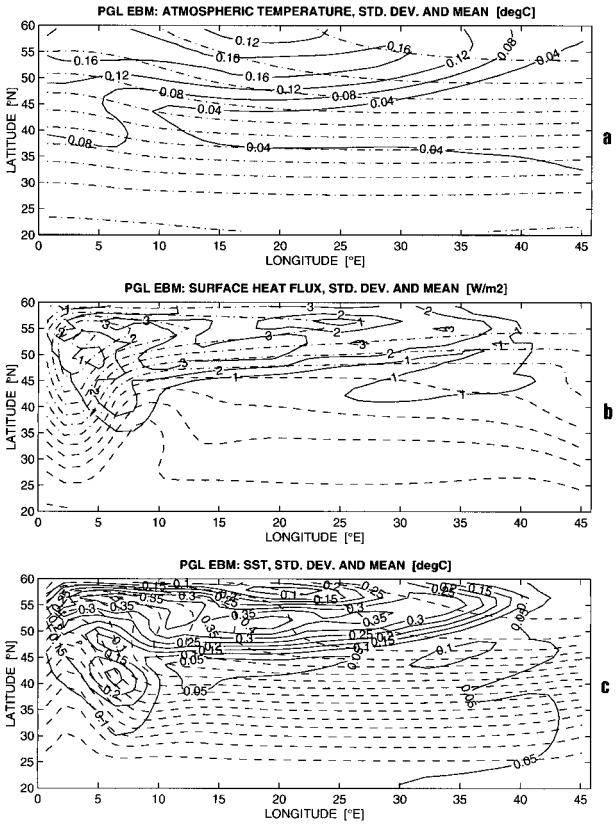

FIG. 3. (a) Time-average (dashed contours) and std dev (solid) of atmospheric temperature, (b) surface heat flux, (c) and SST. Mean contours are every 2°C for atmospheric temperature and SST, every 10 W m^{-2} for the fluxes.

studies in the latitude–depth plane failed to show decadal oscillations. With overturning increasing with temperature (or buoyancy) anomalies, it is readily seen that if for instance the temperature anomaly is larger than at steady state, the overturning is also larger causing a larger advective heat transport that damps the initial temperature anomaly (this will be reexamined in detail in the next section).

In contrast, Drbohlav and Jin (1998, hereinafter DJ) have quite recently produced interdecadal oscillations using a 2D (latitude–depth) ocean model driven by constant flux. The result is puzzling in view of what was just said and also because we know that the essential ingredients, baroclinic instability, and planetary waves are absent in such a geometrical setting. What is then the nature of the oscillations and instability in their 2D model and to which extent is this a good analog of the 3D situation? An answer to this question can be provided by casting their formulation in terms of a two-layer model supposed for simplicity to have a thin upper-thermocline layer h compared to the total depth. Only the baroclinic mode meridional velocity (the velocity difference between the upper and lower layer) is active because the barotropic mode is absent in such a rigid-lid 2D model. According to DJ's dynamics, the equations for the variables h and v can be cast as

$$\frac{Dv}{Dt} = -g'\varepsilon\frac{\partial h}{\partial y} + F, \tag{1a}$$

$$\frac{\partial h}{\partial t} + \frac{\partial}{\partial y}(hv) = Q, \tag{1b}$$

where g' is the reduced gravity and ε a small coefficient used in DJ's semiempirical formulation, Q is the mass flux between the layers that parameterizes heating and cooling, and F represents frictional effects. The novelty here is the presence of inertia in (1a) that introduces a phase lag between the density field and the overturning, which permits oscillations. The small coefficient ε is there to parameterize effects of the earth's rotation.

Suppose that a mean state distribution of velocity and thickness (V, H) has been found to equilibrate a particular (but constant in time) heat flux distribution. The stability of that particular state can then be obtained from the linearized perturbation equations:

$$\frac{\partial v'}{\partial t} = -g'\varepsilon\frac{\partial h'}{\partial y}, \tag{2a}$$

$$\frac{\partial h'}{\partial t} + \frac{\partial}{\partial y}(Hv' + h'V) = 0. \tag{2b}$$

The variables h' and v' are the departures from the mean state and nonlinear and frictional terms have been omitted in (2a) because their presence is not important for the present argument. Eliminating v' between (2a) and (2b) yields

$$\frac{\partial}{\partial t}\left(\frac{\partial}{\partial t} + V\frac{\partial}{\partial y}\right)h' - c^2\frac{\partial^2 h'}{\partial y^2} + \frac{dV}{dy}\frac{\partial h'}{\partial t} = 0. \tag{3}$$

The parameter c is simply $(g'H\varepsilon)^{1/2}$, the phase velocity of the waves that travel along the interface in the absence of a mean flow. Equation (3) is in fact telling us that the waves have the structure of internal gravity waves. Because they are slowed down enormously by the introduction of the ε factor, they enter the range of interdecadal oscillations. Estimating g' as the expansion coefficient (2×10^{-4} K^{-1}) times the thermal contrast between upper and lower layer (6°C), and $H = 500$ m, the true internal gravity wave speed $(g'H)^{1/2}$ is 2.5 m s^{-1}. Using DJ value for ε (1.25×10^{-5}), the wave speed drops to 0.9 cm s^{-1}. Since structures of half a wavelength typically appear in their 6000-km domain, the estimated period of free waves for 12 000-km wavelength is 44 yr, well into the range of interdecadal scales. Of course, the presence of a mean flow modifies this. When the mean flow is constant, the modification reduces to a Doppler shift that alters the real wave speeds. More significantly, the last term in (3) shows that when the mean flow is convergent ($dV/dy < 0$), a linear instability arises whose growth rate is just controlled by the value of the convergence—to see this, balance the

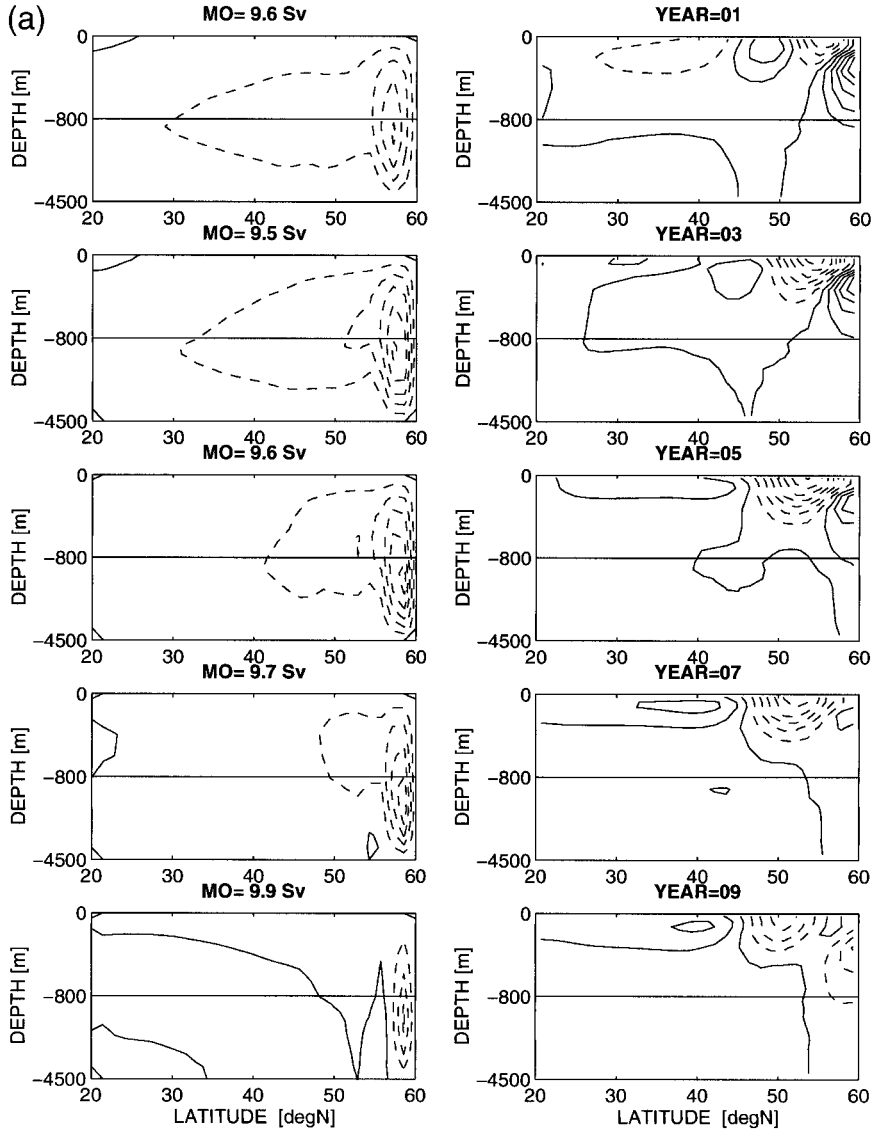

FIG. 4. Meridional overturning anomaly and zonally averaged temperature anomaly for various phases of the oscillation in the 3D coupled model (10 snapshots every 2 yr for the 20-yr oscillation).

first and last term in (3). Consider regions of heat losses ($Q < 0$), where the mean heat (mass) transport $(\partial/\partial y)(HV)$ is convergent. Suppose that the mean depth is perturbed to a slightly larger value (uniformly so that velocities are unchanged), then more heat is brought by the mean flow than can be extracted by the constant forcing and the layer continues to deepen. This is a simple mechanism that could perhaps account for the slow instability witnessed by DJ. Such an effect was mentioned in CVH but was judged to be weak when compared to baroclinic instability in interpreting 3D simulations. It seems therefore that both the oscillations and the instabilities of this 2D model have a physical nature rather different than those observed in OGCMs and it is difficult to qualify this model as a good physical analog.

The anomalies of the overturning and zonally averaged temperature for the 3D model discussed previously (Fig. 4) can be compared with DJ's. While the basin geometry is slightly different as well as the forcing (EBM model vs surface fluxes diagnosed at the end of a restoring run in DJ), significant differences appear in the structure of the anomalies in the 2D and 3D models (in addition to very different oscillation periods, 20 yr vs 65 yr in DJ). While overturning anomalies are limited to the northern 10° of the basin in the 3D model and remain usually of the same sign in the whole basin, DJ's simulation show large variations of the overturning at

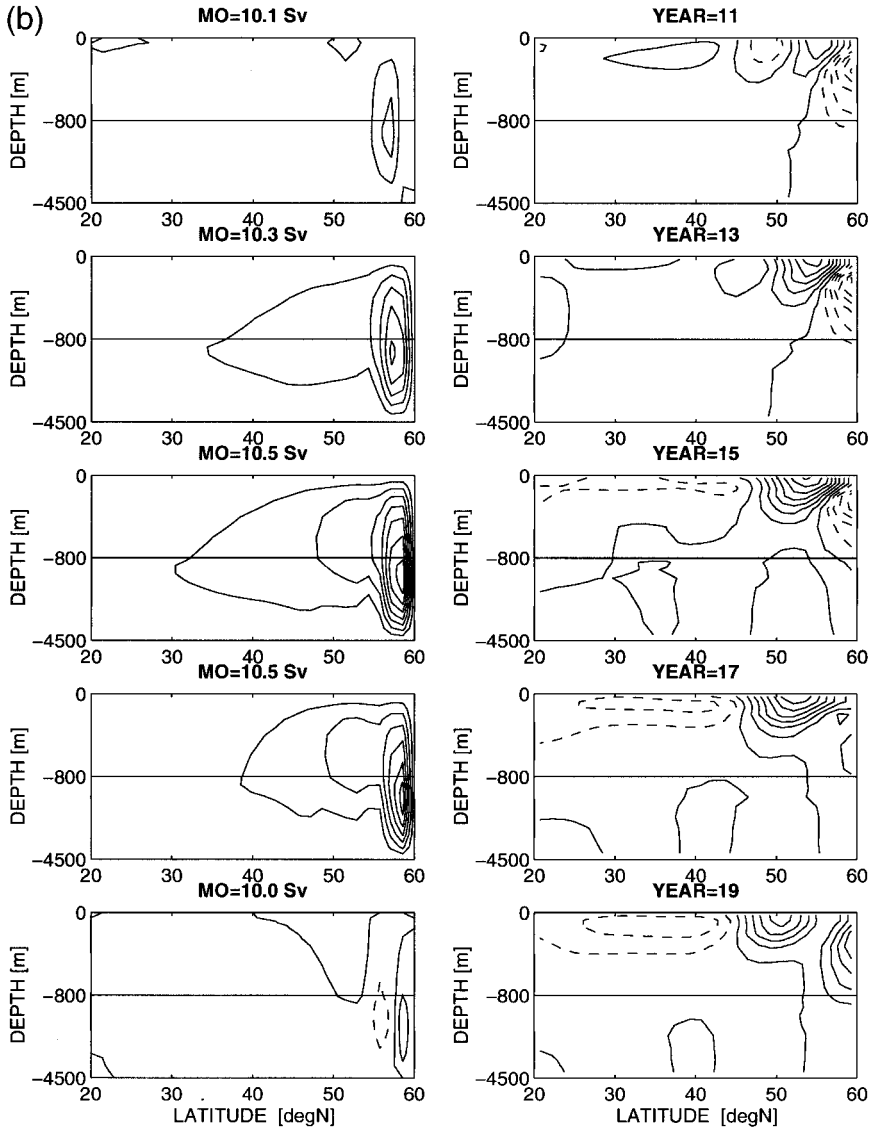

FIG. 4. (*Continued*) Contours are every 0.25 Sv (0.5°C) for the overturning (temperature) anomalies (dashed contours are negative anomalies).

all depths and latitudes, the structure of the anomaly being most of the time bipolar. Temperature variations are intensified in the upper 500 m and in the northern part of the basin in the 3D model, anomalies being usually of one sign. In contrast, the 2D temperature anomalies often show a sign reversal on the vertical, extend all the way from the equator to high latitudes from the surface to 1000 m. Moreover, the phase lag between the meridional density contrast and overturning anomalies is not clear in the DJ model.

4. Formulation of a box model analog

Consider the situation in Fig. 5 where two atmospheric boxes are coupled to two oceanic boxes. The atmospheric boxes exchange heat externally through incident solar flux Q_S and infrared back radiation flux Q_L to outer space. We assume that the heat flux Q_{A0} between ocean and atmosphere is simply equal to $\lambda(T_A - T_O)$, the difference between atmospheric and oceanic temperatures. Because the characteristic timescale of response of the atmosphere to an oceanic temperature anomaly that is in the range of days to weeks is small compared to decadal timescales, it is an excellent assumption to assume that the atmosphere is in energy balance, with the various fluxes adding to zero:

$$Q_S^i - Q_L^i - Q_{A0}^i + K_A(T_A^j - T_A^i) = 0, \qquad (4)$$

where the indices $i = 1, 2$ ($j = 3 - i$) refer to the tropical and polar atmospheric box, respectively. Here K_A is the turbulent eddy heat conductivity that parameterizes lateral eddy transport. For the range of tem-

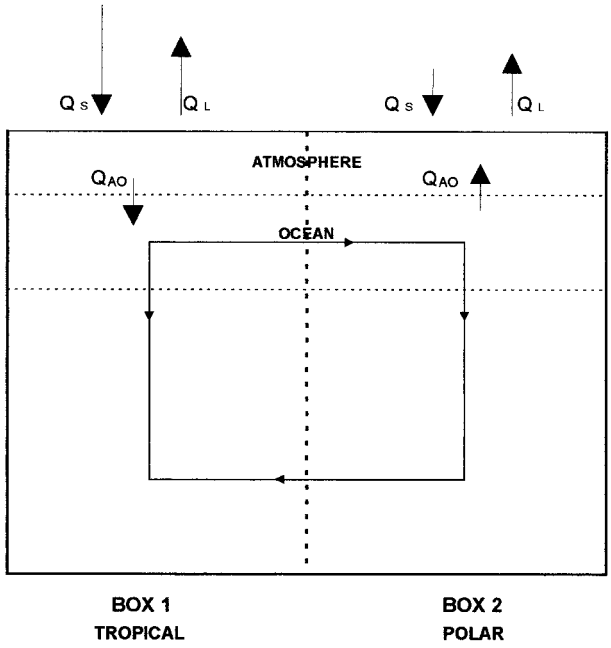

FIG. 5. The geometry of the four-box ocean–atmosphere model. Only the variations of the upper thermocline are considered.

perature variations of interest, the Stefan–Boltzmann's law can be linearized (Budyko 1969) so that

$$Q_L = A + BT_A.$$

Making this substitution in (4) gives an equation for $y = T_A^1 - T_A^2$, the temperature difference between the two atmospheric boxes, in term of $x = T_O^1 - T_O^2$ the temperature difference between the two oceanic boxes:

$$\Delta Q_S - By - \lambda(y - x) - 2K_A y = 0, \qquad (5)$$

where $\Delta Q_S = Q_S^1 - Q_S^2$ is the net differential solar input at the top of the atmosphere. Dependence on absolute temperature drops out in (5) because we have assumed for simplicity the same coefficients A and B for each box for the linearized expression of the infrared flux. This symmetry condition allows us to derive expressions that depend only on the temperature differential between the boxes and not on the mean temperature of the boxes. We are only concerned here with internal redistributions in the ocean–atmosphere system.

Both y and Q_{A0} the flux driving the oceanic boxes can then be expressed in terms of x:

$$y = \frac{\lambda x + \Delta Q_S}{\lambda + B + 2K_A} \quad \text{and} \qquad (6)$$

$$\Delta Q_{A0} = \lambda(y - x) = \frac{\lambda \Delta Q_S}{B + \lambda + 2K_A} - \frac{\lambda(B + 2K_A)}{B + \lambda + 2K_A}x. \qquad (7)$$

Atmospheric temperature anomalies follow closely (and linearly) oceanic temperature anomalies with a ''slope'' $\lambda/(\lambda + B + 2K_A)$ of 0.77 when values of $\lambda = 15$ W m^{-2} K^{-1}, $B = 1.7$ W m^{-2} K^{-1}, and $K_A = 1.3$ W m^{-2} K^{-1} are inserted. The values of B and K_A are those chosen by Marotzke and Stone (1995) in their study of the sensitivity of climate models to flux corrections. The value of λ corresponds to those of Seager et al. (1995); it is well below the threshold beyond which no decadal oscillations exist in CVH's OGCM. The ocean–atmosphere heat flux is dominated by the differential of solar flux, the first term on the rhs of (7) for all reasonable values of oceanic temperature differences. This occurs because the box model captures only the largest scales of spatial variability much larger than the atmospheric diffusive length scale of the order of 700 km, as discussed by Marotzke and Pierce (1997). Equation (7) solves the energy balance of the atmospheric box model by providing the surface flux in terms of oceanic temperatures only.

Turning our attention to the oceanic compartment, two processes are included to transport heat meridionally, turbulent eddies akin to those included in the atmospheric compartment and more importantly the large-scale thermohaline circulation made possible in the ocean by the existence of meridional boundaries. The term ''thermohaline'' is improper in our context since fresh water and salt transports are not considered in this study but we will stick, nevertheless, to this usual convention.

The heat conservation equation for each oceanic box is

$$(\rho C_p h)_0 \frac{\partial T_o^i}{\partial t} = Q_{A0}^i + \left(\frac{\rho C_p}{A}\right)_0 \psi(T_O^j - T_O^i) + K_0(T_O^j - T_O^i), \qquad (8)$$

where h and A (5000 km $\times$ 2000 km) are, respectively, the depth and area of each box, ψ is the overturning stream function (m^3 s^{-1}), and K_0 is the eddy heat conductivity (W m^{-2} K^{-1}). Because decadal oscillations appear as surface intensified phenomena in OGCMs, the subtropical box will be taken to have a depth h of 1000 m, much less than the depth of the ocean. The polar box with active convection should have a much greater depth and connect to deep abyssal boxes, as in HCW. However, if we want to preserve symmetry conditions that allow us to focus on temperature differentials only, we need to have a polar box identical to the subtropical one. Including explicitly a deep abyssal layer would allow us to predict mean temperatures as well. However, the adjustment timescale of the deep ocean is at least one order of magnitude larger than decadal timescales and these processes are purposely filtered out. After introducing a timescale τ (=1 yr) for the time variable, and a scale hA/τ for ψ, (8) can be transformed into an equation for the oceanic temperature difference x between the tropical and polar box:

$$\dot{x} = \alpha\lambda(y - x) - 2\psi x - 2\alpha K_0 x, \qquad (9)$$

where $\alpha = \tau/(\rho C_p h)_0$ is a constant (K m^2 W^{-1}). The

variable y can now be eliminated between (7) and (9) to yield a single equation for x:

$$\dot{x} = q - 2\psi x - \delta x, \tag{10}$$

where the driving flux q is $(\alpha\lambda\Delta Q_S)/(\lambda + B + 2K_A)$ and the diffusion δ is

$$\alpha\left(2K_0 + \frac{2\lambda K_A}{\lambda + B + 2K_A} + \frac{\lambda B}{\lambda + B + 2K_A}\right),$$

summarizing the cumulative effects of eddy heat transports in the ocean and in the atmosphere and infrared back radiation. Lagrangian marker dispersal in the ocean gives eddy diffusivity estimates in the range of 10^3 m^2 s^{-1} that translates to eddy heat conductivities of $10^3 \times (\rho C_p h)_0/L^2$, where the appropriate length scale L over which the diffusion process is analyzed, is made equal to the meridional size of the box. Values for h (L) of 1 km (2000 km), respectively, give $K_0 \sim 1$ W m^{-2} K^{-1}. It is readily seen that the three contributors to the diffusion in (10) have the same order of magnitude, giving an overall diffusion timescale δ^{-1} of 23.7 yr. The remaining contributor to the heat transport that is needed to respond to the differential flux q in the steady state comes from the overturning that adjusts a surface temperature anomaly on a timescale $(2\psi)^{-1} \sim 10$ yr under typical ''present day'' conditions of 15 Sv for the equator-to-pole mass transport. This is twice as efficient as the sum of turbulent diffusion and infrared losses.

A dynamical equation must be added to relate the time rate of change of the overturning and temperature. There are additional feedbacks caused by variations of the eddy diffusivities K_A and K_0 with temperature gradients, but we have decided to concentrate solely upon the overturning. OGCMs readily provide the overturning streamfunction in the latitude–depth plane. The quantity being determined by the zonal pressure gradient, it does not lend itself to easy parameterization in zonally averaged or box models. Originating with Stommel (1961), numerous studies have appeared that ultimately rest upon a steady-state balance between the buoyancy torque proportional to x and dissipation proportional to ψ with no phase lags. The absence of phase lags may well be justified for very long timescales much larger than the decadal scales of baroclinic signals but clearly is inappropriate here, as shown by Greatbatch and Peterson (1996) and CVH. These studies have shown the existence of quadratures that must be included in lower-order models that aim at reproducing the behavior of GCMs. Ruddick and Zhang (1996) recently added support to this requirement by proving the nonoscillatory nature of the original Stommel 1961's box model. A generic form of our dynamical predictive equation for ψ is therefore

$$\dot{\psi} = f(x, \psi).$$

The problem is now to discover the functional dependence $f(x, \psi)$ that reproduces unstable oscillatory fixed points that appear under Hopf-type bifurcations when the diffusion is progressively lowered. The existence of Hopf bifurcations in OGCMs from a steady THC regime to an oscillatory one has been shown by Chen and Ghil (1996) against variations of λ and by CVH against variations of eddy diffusivity. The latter authors showed that this was made possible, first by an instability process concentrated in the western boundary current extension of their oceanic basin (i.e., the regime of baroclinic instability at scales that are large compared to the Rossby radius of deformation) and second by the existence of planetary potential vorticity (PV) modes in the interior. As will be shown next, relatively simple and physically plausible forms for $f(x, \psi)$ allow to recover these 3D effects. It is, of course, illusory to recover the hydrodynamics of oceanic baroclinic instability in a one-layer, two-box fluid model, but its salient physical effects can be parameterized. We present the results voluntarily in an unusual fashion by showing first how a simple functional dependence for $f(x, \psi)$ allows a supercritical Hopf bifurcation of the 2 degree of freedom dynamical system and later justify from a physical point of view the necessarily nonunique form that has been chosen.

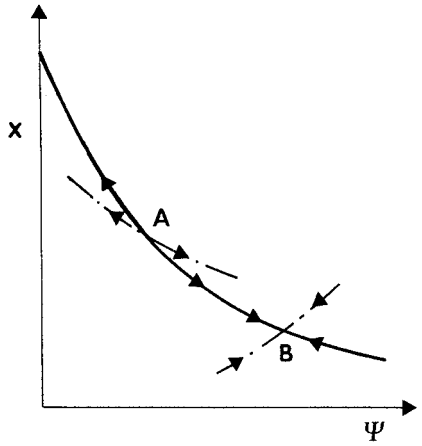

FIG. 6. The variables ψ and x represent, respectively, the oceanic overturning streamfunction and the meridional oceanic temperature contrast. The steady-state curves for temperature (solid) and overturning (dashed) intersect at fixed points, such as A or B. It is readily seen that the system perturbed away from B is driven back to B along either the steady-state temperature curve or the overturning curve. This is not the case at a point such as A, where the perturbations along the steady-state temperature curves are unstable. We propose that the behavior of A-type points is relevant to the existence of decadal oscillations.

Consider the steady-state equation imposed from (10): $x = q/(2\psi + \delta)$. Any point on this curve (Fig. 6) in the x–ψ phase space for which $f(x, \psi)$ vanishes is a fixed point of the dynamical system. The largest x $(=q/\delta)$ value is obtained when ψ is zero. In this diffusive state the heat input is balanced entirely by eddy heat transport and infrared back radiation. A nonzero overturning requires less meridional temperature dif-

ference to balance a given surface flux. In the neighborhood of a fixed point of coordinates ($x_0 > 0$, $\psi_0 > 0$) arbitrary at this point, the linearized equations for the perturbations are

$$\dot{x} = -\frac{q}{x_0}x' - 2x_0\psi',$$

$$\dot{\psi} = \frac{\partial f}{\partial x}x' + \frac{\partial f}{\partial \psi}\psi',$$

in which the f partial derivatives are evaluated at the fixed point. Exponential solutions $e^{\lambda t}$ require the exponent λ to obey

$$\lambda^2 + \lambda\left(\frac{q}{x_0} - \frac{\partial f}{\partial \psi}\right) + 2x_0\frac{\partial f}{\partial x} = 0.$$

The conditions for the fixed point to be a spiral source ($\lambda_R > 0$, $\lambda_I \neq 0$) require

$$\frac{\partial f}{\partial \psi} > \frac{q}{x_0}, \tag{11a}$$

$$\frac{\partial f}{\partial x} > \frac{1}{8x_0}\left(\frac{q}{x_0} - \frac{\partial f}{\partial \psi}\right)^2. \tag{11b}$$

Therefore, a weak but necessary condition for oscillatory instability is that both partial derivatives be positive since q and x_0 are positive by definition. This implies in turn that $(\partial x/\partial \psi)_f$ be negative at the fixed point so that the intersection of the heat curve with the dynamic curve of equation $f(x, \psi) = 0$ must occur with a negative slope as sketched in Fig. 6. This surprising conclusion is opposite to the choices of Stommel's type of parameterizations for which ψ is an increasing function of x and provides the key to the existence of unstable oscillatory states. There are two other elements that help to further select a functional form for f. The first is that we ask the diffusive state to be a fixed point and for this to be the case $f(x, \psi)$ must be of the form $\psi g(x, \psi)$. The oceanic box model has then two equilibria, an advective one with an active meridional thermohaline circulation and a diffusive one in which the heat transport is carried out entirely by the turbulent eddies. In this diffusive mode, the ocean heat transport has physical origins akin to the midlatitude atmospheric heat transport through the ''small-scale'' baroclinic instability of a zonal circulation. The second element is that friction must be active to equilibrate buoyancy torque for large values of ψ. The dynamical system is dissipative and $(\partial\dot{x}/\partial x) + (\partial\dot{\psi}/\partial\psi) < 0$ at large values of x and ψ. This implies that the curve of equation $f(x, \psi) = 0$ pictured in Fig. 6 must change slope for large values of ψ. The simplest continuous curve with a change of sign in slope is a parabola and g is then chosen to be of the form:

$$g(x, \psi) = k(x - x^*) - \gamma(\psi - \psi^*)^2.$$

These considerations lead us to consider as a prototype for interdecadal oscillations the following system:

$$\dot{x} = q - 2\psi x - \delta x, \tag{12a}$$

$$\dot{\psi} = k(x - x^*)\psi - \gamma(\psi - \psi^*)^2\psi, \tag{12b}$$

where k, γ, x^*, and ψ^* are free parameters. A somewhat unusual path has been used to ''find Eq. 12b'' from properties of its solutions. The nonunique choice for f is, of course, highly artificial unless a physical interpretation be given. The first term on the rhs of (12b) tells us that if the north–south temperature contrast exceeds a given bound, then that term is responsible for an exponential increase of ψ. One of the results of the analysis of OGCMs by CVH is that the driving behind the interdecadal oscillations is the baroclinic instability of the mean thermohaline circulation. In that context, the first term in (12b) mimics that instability when potential energy (the x variable) is available to be converted in kinetic energy (the ψ variable). Physically a vertical shear is associated with x trough the thermal wind equation, so that in agreement with baroclinic instability theory, the growth rate is made proportional to that vertical shear. Under this process the meridional circulation is then replenished at a rate controlled by the available potential energy. Of course, it would also be possible to add another feedback by allowing enhanced turbulent diffusion by small-scale baroclinic eddies for larger x, but we have not considered this process at the present stage because the importance of oceanic eddy heat transport has not yet been so clearly confirmed in OGCMs. The presence of a threshold x^* to initiate exponential growth is not essential but is a matter of simplicity. If x^* is absent, the parabola cuts the heat curve at a second fixed point. By our previous arguments, that second fixed point (higher ψ, lower x) is stable (since the slope of the parabola is positive there) and the model state is bound to be attracted asymptotically to that sink. Indeed numerous additional equilibria appear in OGCMs, but mostly in configurations with two active parameters, temperature and salinity. CVH's (temperature only) model results indicate that the absence of oscillations is not caused by a transition to new equilibria, but by increased damping effects such as turbulent diffusion or stiff restoring to a surface temperature distribution. Therefore we use nonzero x^* (and ψ^*) to ensure the existence of a single advective fixed point that necessarily occurs at x (ψ) larger (smaller) than x^* (ψ^*). While little alternative choices exist to parameterize a large-scale baroclinic instability (present at infinitesimal amplitudes), there is definitely more arbitrariness in the choice of the friction term. Yet the choice made is the simplest one within the domain of functions with continuous derivatives. It ensures dissipation of the dynamical system by saturating the amplitude of the unstable perturbations. Precisely and only at the fixed point, buoyancy torque balances the friction as in Stommel's (1961).

One might object to the formulation of the friction term on the basis that equilibrium solutions of OGCMs tend to have overturning varying linearly with imposed

surface temperature contrast. The present formulation with fixed values of x^* and ψ^* provides a steady-state overturning varying as the square root of the atmospheric temperature contrast in place of the linear law. However, it is clearly unphysical to vary the surface boundary conditions and keep restoring the same (x^*, ψ^*) state. The proper variation of overturning against externally imposed temperature contrast must go along with adequate variations of x^* and ψ^*. Consequently, we can use the model only locally in parameter space to understand the conditions under which decadal oscillations appear around a fixed point for given values of x^* and ψ^*.

One last comment is that (12b) is Landau's equation, an equation used to describe the transition to turbulence through hydrodynamic instabilities. Landau used that equation in its simplest form to show that at a critical Reynolds number, the system could bifurcate along the road to turbulence from a laminar flow to a time-dependent periodic one (see Drazin and Reid 1981 for a review).

5. Stability and oscillatory states

We now proceed to examine in detail the properties of (12a)–(12b). First of all, in order to have a single fixed point (in addition to the diffusive one) in the situation of Fig. 6, the parabola must intersect the $\psi = 0$ axis below the diffusive equilibrium temperature contrast q/δ and its minimum must be above the heat curve, requirements for the parameters that translate into

$$\frac{q}{2\psi^* + \delta} < x^* < \frac{q}{\delta} - \frac{\gamma}{k}\psi_*^2. \tag{13}$$

These inequalities will be assumed to hold in what follows and under these conditions the two fixed points are

$$(x, \psi) = \left(\frac{q}{\delta}, 0\right)$$

the diffusive state, while the second ''advective'' fixed point is solution of the cubic

$$2\psi^3 + (\delta - 4\psi^*)\psi^2 + 2\left(\psi^{*2} - \delta\psi^* + \frac{k}{\gamma}x^*\right)\psi + \frac{k}{\gamma}(x^*\delta - q) + \delta\psi^{*2} = 0. \tag{14}$$

At most one real root is solution of (14) under conditions (13). Instability of the fixed points depends on condition (11a), which becomes

$$\frac{q}{x} - k(x - x^*) < \gamma(\psi^* - \psi)(3\psi - \psi^*). \tag{15}$$

This condition can be quickly recovered by forming the divergence of (12):

$$\frac{\partial \dot{x}}{\partial x} + \frac{\partial \dot{\psi}}{\partial \psi} = -2\psi - \delta + k(x - x^*) + \gamma(\psi^* - \psi)(3\psi - \psi^*). \tag{16}$$

At a fixed point, $2\psi + \delta$ is just q/x and the condition of a positive divergence is identical with (15). The oscillatory nature of the dynamical system depends on whether the divergence takes both signs in the x–ψ plane, a necessary condition known as the Poincaré–Bendixon theorem. It is immediately fulfilled when the instability condition (15) is met because (16) shows that the divergence becomes negative for large values of ψ (for a given x), a condition that shows the dissipative nature of the system. The condition for imaginary exponentials (11b) is easily obtained from the linear stability analysis.

In the exploration of parameter space, the values of x^* and ψ^* have been fixed. The parameter k bears upon the timescale of the oscillations, as can be inferred from (11b). It is linked to the phase lag that exists in the ocean between the western boundary current transport and the interior temperature gradient lag that depends on the time it takes for a planetary wave to cross the basin (HCW). Only the friction γ and the diffusion δ are varied in the parameter space exploration that is presented next. Fixed parameter values are $k = 0.1$ yr^{-1} K^{-1}, $\psi^* = 15$ Sv, $x^* = 11.715$ K, and $\Delta Q_S = 200$ W m^{-2}. The oceanic boxes extend 5000 km (2000 km) in longitude (latitude) and are 1000 m deep. The real part of the eigenvalues (i.e., the growth rates) near the diffusive and advective fixed points are shown in Fig. 7 with respect to γ and δ. The growth rates near the diffusive fixed point are positive (negative) for small (large) δ. With the value of δ previously estimated, the diffusive solution is unstable almost independently of the value of γ. It can also be shown that it is nonoscillatory. Since the temperature contrast of the diffusive solution is much larger than x^*, positive ψ perturbations are rapidly amplified. The analysis in the neighborhood of the advective fixed point shows that its stability boundaries are more complex. For each γ there are limits in δ beyond which (14) has either two roots or no root. Only the domain inside the limits given by (13) has been explored. First, γ must exceed a certain cutoff value for the fixed point to be unstable for a given δ. Conversely, for γ above this cutoff, the fixed point is stable for sufficiently low and sufficiently high δ values. The former limit is counterintuitive. It comes from the fact that as δ decreases to low values, ψ increases and x decreases in a combination that makes the system more dissipative. At the difference of the diffusive case, larger temperature contrast and smaller overturning are now obtained for larger diffusion and friction. In the whole domain of existence of this fixed point, the perturbation solutions are oscillatory. Their frequency depends weakly on γ and decreases with increasing diffusion, as expected.

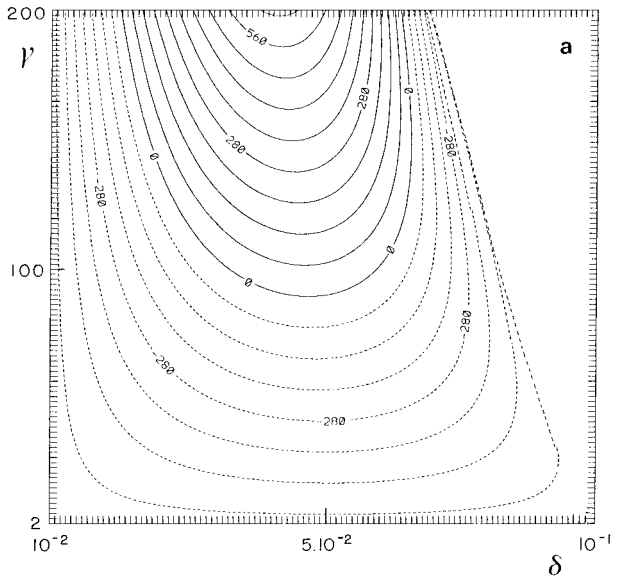

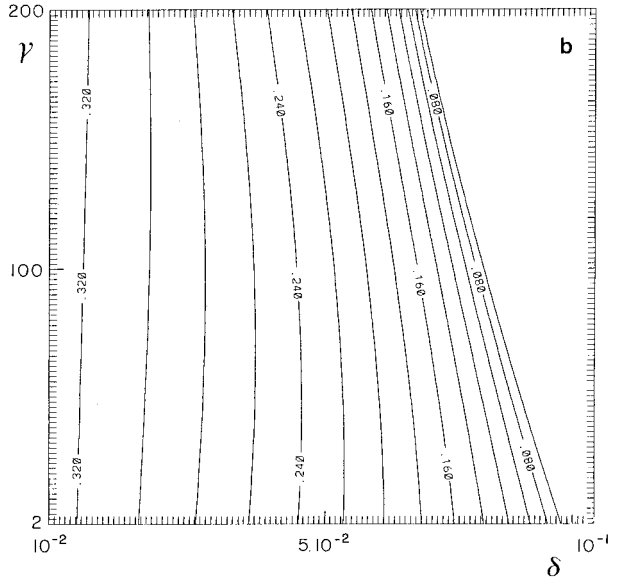

FIG. 7. The real part of eigenvalues at the advective (diffusive) fixed points are shown in (a) [(b)] in the δ (diffusion), γ (friction) parameter space. The diffusive state is always unstable while for large γ a "window" of δ values allows instability of the advective fixed point. It is in the positive (solid contour) region of (a) that a supercritical Hopf bifurcation is possible. The contour interval values are multiplied by 10^4 in (a). They are, respectively, 7×10^{-2} yr^{-1} and 2×10^{-2} yr^{-1} for (a) and (b). (The δ values are in yr^{-1} and γ values when multiplied by 10^{-5} are in Sv^{-2} yr^{-1}.)

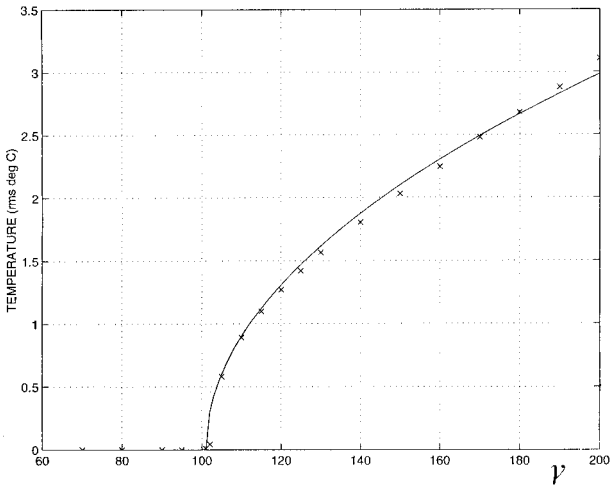

FIG. 8. The bifurcation diagram of the temperature oscillations (rms measure) is shown against γ (friction parameter). At γ_c the system is unstable and a limit cycle develops (γ values multiplied by 10^{-5} are in Sv^{-2} yr^{-1}).

It is now possible to turn to the temporal description of particular solutions. With the diffusion $\delta = 4.2 \times 10^{-2}$ yr^{-1} previously estimated, and k (=0.1 K^{-1} yr^{-1}) typical of the sensitivity observed in OGCMs, Fig. 8 shows the rms amplitudes of the temperature perturbations at large times as functions of γ. It is surprising at first to see the perturbations growing with an increase in the friction parameter γ. This comes from the fact that as γ increases, the distance of the fixed point ψ_0 to ψ^* diminishes. The square of that distance appears in the friction parameterization and this effect overrules the increase in γ so that the net friction near the fixed point decreases. For values of γ larger than γ_c (=9.97 $\times 10^{-4}$ Sv^{-2} yr^{-1}), the fixed point becomes unstable in an oscillatory manner at a value predicted by the linear analysis (15). The dependence of amplitudes of the limit cycle on $(\gamma - \gamma_c)^{1/2}$ is the familiar signature of a supercritical Hopf bifurcation at γ_c. Equation (11a) shows that the critical condition at bifurcation gives $\partial f/\partial\psi$ equals q/x_0 (=1.22/12.02), implying an exponential amplification of ψ in slightly less than 10 yr. We recover the kind of efficiency measured by the parameter μ in CVH. With values of γ only 3.5% above critical, small perturbations grow over a 2000-yr timescale to finite amplitudes of 0.22°C (0.4 Sv) with oscillations of about 25-yr period around the advective fixed point at 12.03°C (9.47 Sv). The nearly sinusoidal shape and the amplitudes of these oscillations, the phase lag between the temperature contrast, and the overturning (Fig. 9) all compare very favorably with those observed in the 3D model of section 2. The growth rate is much smaller than the period (23 yr) by almost two orders of magnitude because of the proximity of the bifurcation. Note again the similarities with the 3D simulation that took nearly 5000 yr to reach a quasiperiodic state. (Of course, the initial convergence to the limit cycle can be much more rapid if the perturbations are stronger.) The temperature perturbations in the atmospheric box are always in phase with oceanic temperatures (6)—a result that comes from the weak assumption of low thermal inertia of the atmosphere at decadal scales. For the parameters chosen, their amplitudes are about three-quarters of the oceanic temperatures. Very similar phase and amplitudes were obtained in the coupled 3D model, with the

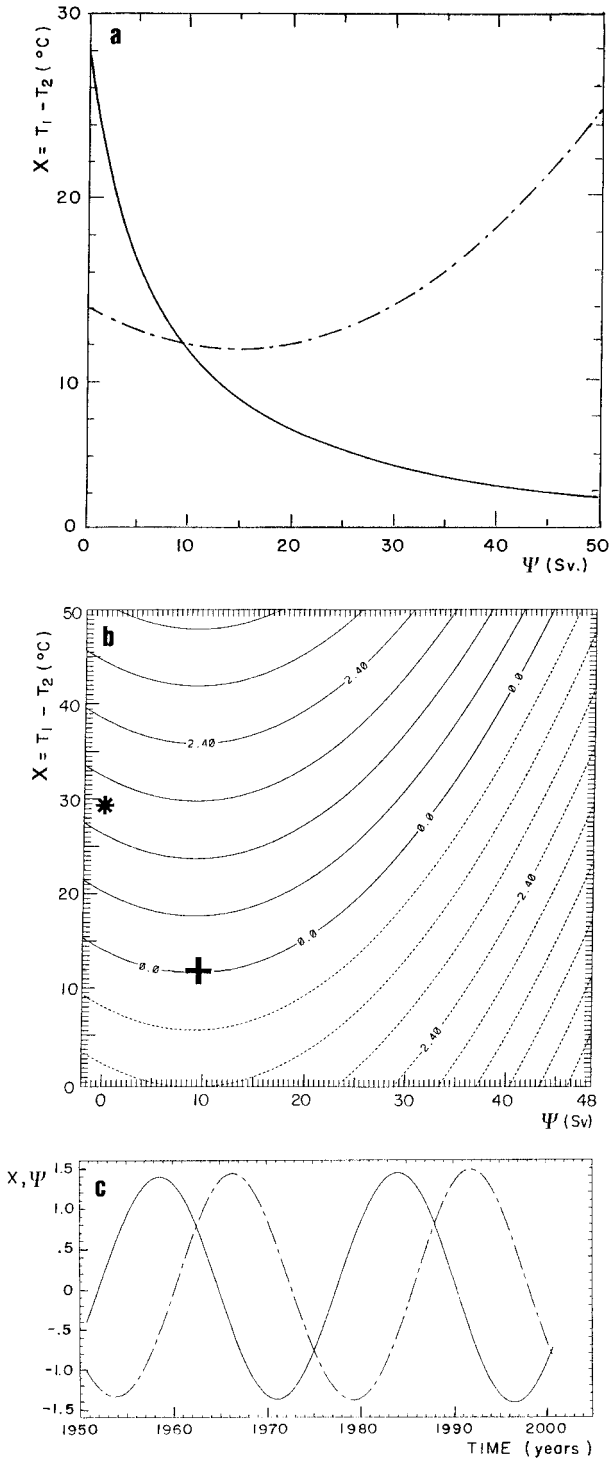

FIG. 9. The solutions are shown for a γ value 3.5% above critical. (a) The steady-state curves that apply in this case are shown. The point of intersection is unstable in the manner of the point A in the sketch of Fig. 5. (b) The divergence in the x–ψ space (positive–solid) along with the position of the diffusive (*) and advective fixed point (+) is shown. (c) The (scaled) oscillations of temperature (solid) and overturning (dashed) in the regime of limit cycle amplitudes similar to those in the coupled 3D model are shown.

rms atmospheric surface temperature reaching in that case 61% of the rms SST. The surface heat flux differential applied to the oceanic box is nearly constant at about 57% of the solar flux differential at the top of the atmospheric box. While OGCMs have been run for a long time with a restoring boundary condition on surface temperature, more recent computations either with constant surface flux or coupling to atmospheric energy balance models have revealed the emergence of decadal oscillations. The nearly constant surface flux of this coupled box model that captures but the largest scales of variability shows the relevance of the simple constant flux experiments. To further appreciate that the model is a physical analog of the behavior of OGCMs we have studied the effect of a switch to restoring boundary conditions. We know from (6) the atmospheric temperature contrast y_O that is prevalent at the advective fixed point. When the limit cycle is well established, we suddenly freeze the atmosphere by fixing y to y_O in (9). The oscillations are now observed to be strongly damped and the system converges back to the advective fixed point in less than 100 yr. This result that agrees with OGCM transitions is not difficult to understand. When y is fixed, the heat equation has the same form as (10), but with a new repartition between forcing and diffusion leading to different values of q and δ. The damping that comes from the diffusion δ increases to a value α ($K_O + \lambda$), a factor of 3.2 larger than the diffusion of the free atmosphere case for the values of the chosen parameters. The diffusion of the frozen atmosphere case can be shown to reach the much lower diffusion of the free atmosphere only at the price of reducing the air–sea exchange coefficient λ to values that are small compared to $B + 2K_A$.

It appears that this 2 degree of freedom climate model reproduces very well the decadal oscillations observed in the three-dimensional model of section 2. To evaluate if this success persists farther away from bifurcation, the oscillations are shown in Fig. 10 at a value 50% above bifurcation. The oscillation now exhibits a definite nonlinear character; the temperature rise significantly slows down with the overturning staying at low values for a larger fraction of the period. The linear rise is increasingly controlled by the sole surface flux. At a given temperature threshold, the overturning rises abruptly, with the instability term in (12b) exceeding the frictional term. In addition the temperature starts to decrease quickly since the advection works to eliminate the temperature contrast. The instability term in (12b) falls below the threshold and ψ starts to decrease, but less rapidly to low values. During the long diffusive rise that follows, the instability and frictional terms remain small. Unfortunately, the 3D oscillations have nonlinear modulations different from the box model oscillations (cf. Figs. 2 and 9a). The increasingly short (long) period of rising of temperature (overturning) in the 3D model is just the opposite of what they are in the box model.

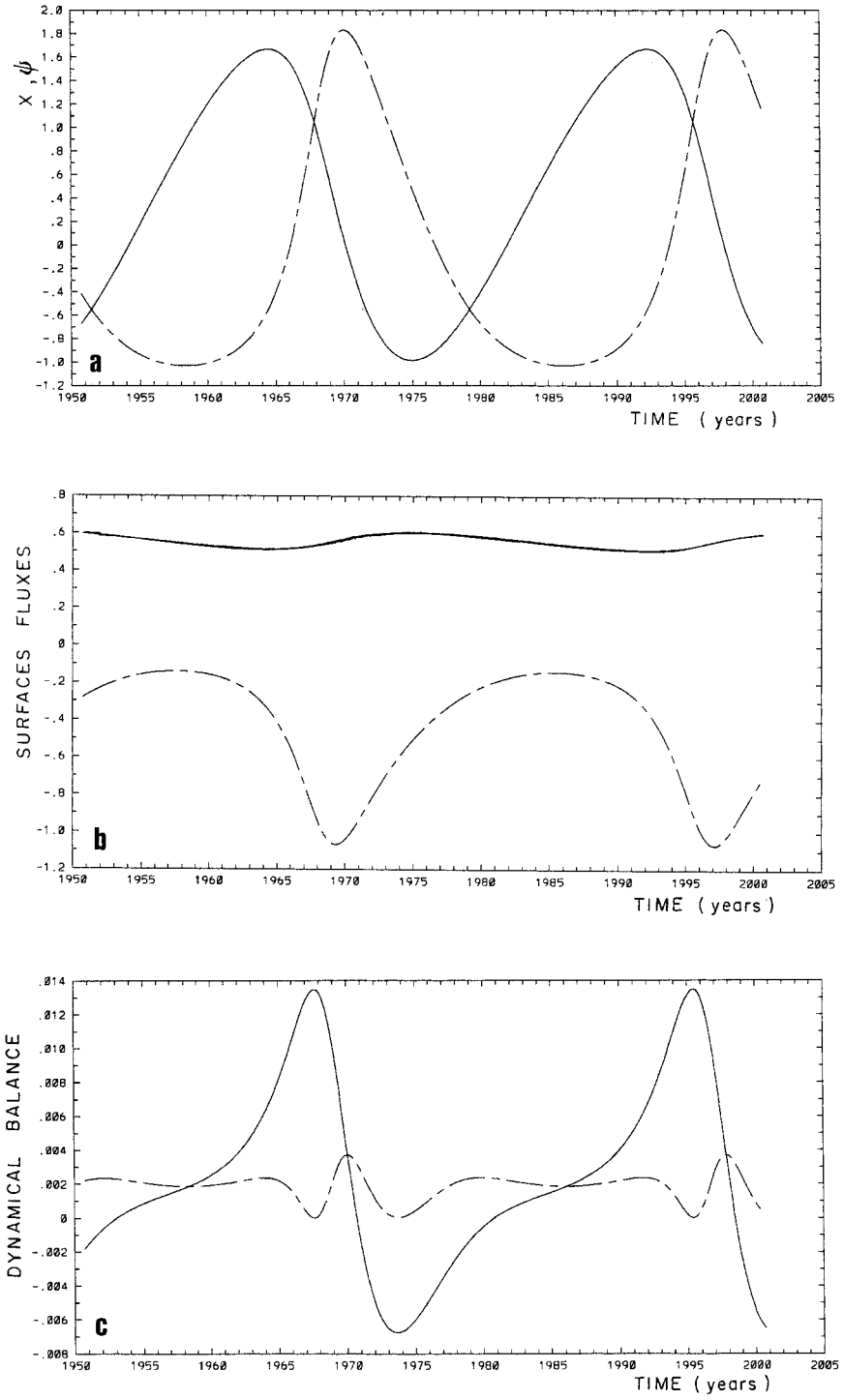

FIG. 10. (a) Temperature (solid), overturning (dashed) are shown in the nonlinear regime at γ values 50% above critical. (b) The surface flux (solid) and advective flux (dashed) of equation (12a) are shown. (c) The instability term (solid) and friction (dashed) of equation (12b) are shown. Note the linear temperature rise that occurs in response to the surface flux when the overturning is small for a large fraction of the period and the steplike behavior of the instability that arises at a given threshold. The rise in ψ is then followed by an almost equally rapid decrease (due to the friction term).

6. Further comparisons with the 3D coupled ocean–atmosphere model

The parameterization of the box model provides a simple framework for the existence of oscillations that may be useful for conceptual purposes. Its strength, if any, must come from a comparison with three-dimensional models. Some important features such as the transition from steady to oscillatory states through supercritical Hopf bifurcations (Chen and Ghil 1996; CVH) are built in our box model parameterization. We have shown that the variations of parameters in the two-box model follow qualitatively what happens in the 3D model and we believe that the success of this parametrization is due to the nearly linear regime of the decadal oscillations in the coupled 3D model. In spite of obvious differences at finite amplitudes if we insist that the important variables that govern the 3D oscillations are the north–south temperature contrast and the overturning stream function, we could estimate these variables in the coupled model simulation (section 2) and check whether their rates of changes are governed by relationships similar to the box model equations (12).

Although the parameterization of the box model is apparently not fully adequate to describe the (nonlinear) regimes of the coupled model, we have tried to estimate the coefficients of the box model parameterizations from the times series of the variables x and ψ *as observed in the coupled model*. Knowing both the variables and their time rates of change, we write for instance an estimate Z_i of $\dot{\psi}/\psi$ as the linear combination at each time step i:

$$Z_i = ax_i + b\psi_i + c + d\psi_i^2.$$

The unknown coefficients (a, b, c, d) are estimated by minimizing the mean-square difference between the observed $\dot{\psi}/\psi$ and the estimator Z_i. The coefficients of the box model that best describe the coupled model behavior can then be obtained. Because there is a significant model trend over the 6000 yr of the experiment, the optimal fits were done on each 1000-yr-long time slices. Overall the parameterization captures most of the variations of $\dot{\psi}$. The estimated k and x^* show some consistency between different time slices while γ and ψ^* are not very well constrained (even the sign of γ changes). The correlation coefficients between $\dot{\psi}/\psi$ and each term of the parameterizations support a tight fit with x while the frictional processes appear as secondary influences. The optimal values of the box model parameters averaged over the six independent time periods are $k = 0.19\ \text{yr}^{-1}\ \text{K}^{-1}$, $x^* = 3.65$ K, $\psi^* = 9.75$ Sv, $\gamma = 1.7 \times 10^{-5}\ \text{Sv}^{-2}\ \text{yr}^{-1}$, the last two showing much uncertainty (in fact the value for γ is negative for the latest periods with the best fit, suggesting that the frictional parameterization is the less satisfying).

The same procedure is applied to the temperature equation. It is only in the last 2000 yr that the box model parameterizations captures most of the variation of x, when the mean state does not evolve anymore. The most robust elements of the parameterization are the constant heat flux and the dependence on ψx (which is better suited than a dependence in ψ alone). On the other hand, the horizontal diffusion factor is not well defined whether in sign or amplitude.

7. Conclusions

Although it has been possible for box models to help in a physical understanding of the multiple steady states of the thermohaline circulation (Stommel 1961), this was not the situation for decadal to interdecadal oscillations. We propose a climate model without hydrological cycles and salinity effects that exhibits a regime of self-sustained oscillatory solutions in the two-boxes category. It relies on a new physical mechanism: when the available potential energy in the ocean exceeds a given threshold, a baroclinic instability develops that feeds the kinetic energy of the overturning circulation. The increased heat transport by the overturning then restores the available potential energy toward its original value. However, the system does not converge to a steady state because of the existence of phase lags between the overturning and the available potential energy. The existence of such phase lags was proposed by HCW to be caused by the finite propagation speed of planetary waves in the oscillatory states of OGCMs, and the instability mechanism has been attributed by CVH to the baroclinic instability of the oceanic circulation in regions of highest vertical shear that usually coincide with those of highest heat losses to the atmosphere.

We have proposed to parameterize this mechanism by using Landau's equation for the overturning and given the general conditions under which the system can oscillate. A Hopf-type bifurcation to a limit cycle exists in the parameter space appropriate to the present state of the ocean–atmosphere system. On these timescales, which are long in comparison with atmospheric adjustment timescales, the role of the atmosphere is one of passive adaptation to the ocean state. In agreement with GCM behavior, it is demonstrated that a switch of the model to restoring boundary conditions to a frozen atmosphere drives the model solution back to steady state because of increased damping. The very good agreement that exists between the box model and the 3D model at small amplitudes does not extend, however, to the nonlinear regime. The oscillations of the temperature contrast in the box model show a marked asymmetry of evolution toward a sawtooth pattern (slow rise, more rapid decline) while the overturning remains at large amplitudes for a shorter fraction of the period. This behavior differs from that of the same variables observed in the coupled PGL–EBM model with a rapid rise of the temperature contrast followed by a slower decline. Given the results of the fit that was carried out between the coupled model variables and the box model equations, we may suspect that the reasons for the different behaviors may originate from an incorrect pa-

rameterization of the dissipation and diffusion processes, because the fit was particularly poor for these processes.

We have refrained, thus far, from commenting on the possible applications of the present study to the observations of the climate system. Because the observed signals at decadal periods are a small fraction of the mean signals, the proposed physical analog that works well in the linear regime could be relevant. Although there is strong evidence from coupled model studies that the ocean can integrate the high frequency stochastic surface forcing to generate a continuous red spectrum, we feel that it is certainly too early to say that this is the only cause of decadal variability in the climate system. A consequence of the present study is to show the great sensitivity of the thermohaline circulation to the value of the appropriate friction coefficient caused by the proximity of the bifurcation point. Direct applications would require a dissipation estimate for the overturning that is obviously lacking at the moment. An immediate concern is to improve the comparison between zonally averaged and 3D models in the nonlinear regime, an objective that brings us back to the closure problem for the zonally averaged thermohaline circulation at decadal periods, a closure necessarily different from that at steady state.

Maas (1994) proposed low-order model equations that were derived from an angular momentum principle. He kept the inertial terms and obtained a system with 3 degrees of freedom for the zonal, meridional, and vertical density gradients. With this added freedom the system exhibited chaos, but Maas pointed out to a state of 500-yr period, self-sustained oscillations with the actual parameter values of the ocean. It would be interesting to compare his model with ours in the future, focusing specifically on decadal oscillations. In the meantime, we feel that it is appropriate to analyze the oscillations found in coupled ocean–atmosphere models to check whether the instability mechanism exploited here that appears to summarize the linear regimes of simplified coupled ocean–atmosphere (PGL–EBM) simulations might also be relevant in situations of much higher complexity.

REFERENCES

Birchfield, G. E., 1989: A coupled ocean–atmosphere climate model: Temperature versus salinity effects on the thermohaline circulation. *Climate Dyn.,* **4,** 57–71.

Bryan, F., 1986: High-latitude salinity effects and interhemispheric thermohaline circulations. *Nature,* **323,** 301–304.

Budyko, M. I., 1969: The effect of solar radiation variations on the climate of the Earth. *Tellus,* **21,** 611–619.

Cai, W., R. J. Greatbatch, and S. Zhang, 1995: Interdecadal variability in an ocean model driven by a small, zonal redistribution of the surface buoyancy flux. *J. Phys. Oceanogr.,* **25,** 1998–2010.

Capotondi, A., and W. R. Holland, 1997: Decadal variability in an idealized ocean model and its sensitivity to surface boundary conditions. *J. Phys. Oceanogr.,* **27,** 1071–1093.

Chen, F., and M. Ghil, 1996: Interdecadal variability in a hybrid coupled ocean–atmosphere model. *J. Phys. Oceanogr.,* **26,** 1561–1578.

Colin de Verdière, A., and T. Huck, 1999: Baroclinic instability: An oceanic wavemaker for interdecadal variability. *J. Phys. Oceanogr.,* **29,** 893–910.

Delworth, T. L., and R. J. Greatbatch, 2000: Multidecadal thermohaline circulation variability excited by stochastic surface flux forcing. *J. Climate,* **13,** 1481–1495.

——, and M. E. Mann, 2000: Observed and simulated multidecadal variability in the North Atlantic. *Climate Dyn.,* in press.

——, S. Manabe, and R. J. Stouffer, 1993: Interdecadal variations of the thermohaline circulation in a coupled ocean–atmosphere model. *J. Climate,* **6,** 1993–2011.

Deser, C., and M. L. Blackmon, 1993: Surface climate variations over the North Atlantic Ocean during winter: 1900–1989. *J. Climate,* **6,** 1743–1753.

Drazin, P. G., and W. H. Reid, 1981: *Hydrodynamic Stability.* Cambridge University Press, 519 pp.

Drbohlav, J., and F. F. Jin, 1998: Interdecadal variability in a zonally averaged ocean model: An adjustment oscillator. *J. Phys. Oceanogr.,* **28,** 1252–1270.

Greatbatch, R. J., and S. Zhang, 1995: An interdecadal oscillation in an idealized ocean basin forced by constant heat flux. *J. Climate,* **8,** 81–91.

——, and K. A. Peterson, 1996: Interdecadal variability and oceanic thermohaline adjustment. *J. Geophys. Res. (Oceans),* **101,** 20 467–20 482.

Griffies, S. M., and E. Tziperman, 1995: A linear thermohaline oscillator driven by stochastic atmospheric forcing. *J. Climate,* **8,** 2440–2453.

Huang, R. X., and R. L. Chou, 1994: Parameter sensitivity of the saline circulation. *Climate Dyn.,* **9,** 391–409.

Huck, T., A. Colin de Verdière, and A. J. Weaver, 1999a: Interdecadal variability of the thermohaline circulation in box-ocean models forced by fixed surface fluxes. *J. Phys. Oceanogr.,* **29,** 865–892.

——, A. J. Weaver, and A. Colin de Verdière, 1999b: On the influence of the parameterization of lateral boundary layers on the thermohaline circulation in coarse-resolution ocean models. *J. Mar. Res.,* **57,** 387–426.

Hurrell, J. W., and H. van Loon, 1997: Decadal variations in climate associated with the North Atlantic oscillation. *Climatic Change,* **36,** 301–326.

Kushnir, Y., 1994: Interdecadal variations in North Atlantic sea surface temperature and associated atmospheric conditions. *J. Climate,* **7,** 141–157.

Maas, L. R. M., 1994: A simple model for the three-dimensional thermally and wind-driven ocean circulation. *Tellus,* **46A,** 671–680.

Mann, M. E., R. S. Bradley, and M. K. Hughes, 1998: Global-scale temperature patterns and climate forcing over the past six centuries. *Nature,* **392,** 779–787.

Marotzke, J., 1990: Instabilities and multiple equilibria of the thermohaline circulation. Ph.D. thesis, Institut für Meereskunde, Christian-Albrechts Universität, Kiel, Germany, 126 pp.

——, and J. Willebrand, 1991: Multiple equilibria of the global thermohaline circulation. *J. Phys. Oceanogr.,* **21,** 1372–1385.

——, and P. H. Stone, 1995: Atmospheric transports, the thermohaline circulation, and flux adjustments in a simple coupled model. *J. Phys. Oceanogr.,* **25,** 1350–1364.

——, and D. W. Pierce, 1997: On spatial scales and lifetime of SST anomalies beneath a diffusive atmosphere. *J. Phys. Oceanogr.,* **27,** 133–139.

——, P. Welander, and J. Willebrand, 1988: Instability and multiple steady states in a meridional plane model of the thermohaline circulation. *Tellus,* **40A,** 162–172.

Rahmstorf, S., 1993: A fast and complete convection scheme for ocean models. *Ocean Modelling,* **101,** 9–11.

Ruddick, B., and L. Zhang, 1996: Qualitative behavior and nonoscillation of Stommel's thermohaline box model. *J. Climate,* **9,** 2768–2777.

Seager, R., Y. Kushnir, and M. A. Cane, 1995: On heat flux boundary conditions for ocean models. *J. Phys. Oceanogr.,* **25,** 3219–3230.

Stommel, H., 1961: Thermohaline convection with two stable regimes of flow. *Tellus,* **13,** 224–230.

Sutton, R. T., and M. R. Allen, 1997: Decadal predictability of North Atlantic sea surface temperature and climate. *Nature,* **388,** 563–567.

Weaver, A. J., and E. S. Sarachik, 1991: Evidence for decadal variability in an ocean general circulation model: An advective mechanism. *Atmos.–Ocean,* **29,** 197–231.

——, J. Marotzke, P. F. Cummins, and E. S. Sarachik, 1993: Stability and variability of the thermohaline circulation. *J. Phys. Oceanogr.,* **23,** 39–60.

Welander, P., 1982: A simple heat–salt oscillator. *Dyn. Atmos. Oceans,* **6,** 233–242.

Winton, M., 1996: The role of horizontal boundaries in parameter sensitivity and decadal-scale variability of coarse-resolution ocean general circulation models. *J. Phys. Oceanogr.,* **26,** 289–304.

Wright, D. G., and T. F. Stocker, 1991: A zonally averaged model for the thermohaline circulation. Part I: Model development and flow dynamics. *J. Phys. Oceanogr.,* **21,** 1713–1724.

——, C. B. Vreugdenhil, and T. M. C. Hughes, 1995: Vorticity dynamics and zonally averaged ocean circulation models. *J. Phys. Oceanogr.,* **25,** 2141–2154.